

APPENDIX G GEOLOGIC HAZARD SCREENING AND EVALUATION EXAMPLES

G-1. Example 1 - Surface Fault Rupture Hazard Screening and Evaluation

This example illustrates the steps involved in screening a site for a surface fault rupture hazard and a subsequent site evaluation using the criteria described in paragraphs F-3 and F-4. The example given below is based on a case history study for an existing building.

a. Review of available information

The building site is located within a developing metropolitan area in a tectonically active region. Twelve moderate- to large-magnitude earthquakes have occurred in the region surrounding the site within the last 160 years. The building is a 137-m (450-foot) long by 61-m (200-foot) wide, one- to two-story structure.

(1) Geotechnical investigations indicated that the site is underlain by volcanic (basalt) and sandstone materials located within a meter of the ground surface. Based on these studies, the original building design called for the building to be supported on shallow foundations extending to bedrock, which was reported to occur close to the surface beneath the building footprint. However, during construction of the foundations in the western part of the building, no rock or rock-like materials were encountered, requiring design and utilization of deep auger cast-in-place piles in this part of the building.

(2) Examination of as-built construction documents indicated the possible presence of an abrupt interface between the rock subsurface conditions to the east and deep soil conditions to the west on the property. When plotted on a map (Figure G-1), these data supported the presence of a steeply dipping rock/soil contact that extended across the site on a north-northwesterly alignment. This trend is consistent with the orientation of known active faults within the site's tectonic environment and also with the direction of the channel of a nearby river.

b. Fault rupture hazard screening

Based on the data available in the geotechnical reports and the construction documents, it was not possible to judge whether the apparent soil/rock contact was a buried erosional channel margin, reflecting a former position of the river, the manifestation of geologically young faulting with a down-on-the-west dip-slip component, or the result of some other process. To

evaluate the possibility of active faulting beneath the site, a surface fault rupture hazard screening was performed.

(1) The screening consisted of the three steps outlined in paragraph F-3. First, geological maps from the U.S. Geological Survey, the state geologic survey, and the county were reviewed. These maps showed that the site is located on a gentle, west-plunging anticlinal fold that was not interpreted to be cut by faults. The maps did reveal, however, the presence of an active, northwest-trending fault within 0.6 miles (1 km) west of the site and another potentially active fault within 0.6 miles (1 km) north of the site. The potentially active fault is not well expressed topographically, and it appeared not to cut deposits interpreted to be of Holocene age (last 11,000 years) but does displace rocks of Quaternary age (last 1.8 million years). Secondly, a review of topographic maps of the site and vicinity revealed no features suggestive of a fault-related origin beneath the site. Third, black and white aerial photographs of the building and vicinity, flown prior to site modification by grading, were examined stereographically. The photos confirmed the presence of the anticlinal fold, but soil cover at the site obscured any fault-related dislocations that might be present in the volcanic layers beneath the site.

(2) The screening process yielded no evidence that faults were present beneath the site. However, the close proximity of a known active fault west of the site having a nearly identical trend to the inferred soil/rock boundary beneath the western part of the building, as well as the close proximity of a fault north of the site that displaced Quaternary-aged sediments, meant that the possibility of a surface fault rupture hazard could not be ruled out. Therefore, further evaluation of the potential for surface fault rupture at the site was performed.

c. Fault rupture hazard evaluation

An exploratory trench was excavated to a depth of 6 to 9 feet (1.8 to 2.7 m) across a portion of an open field

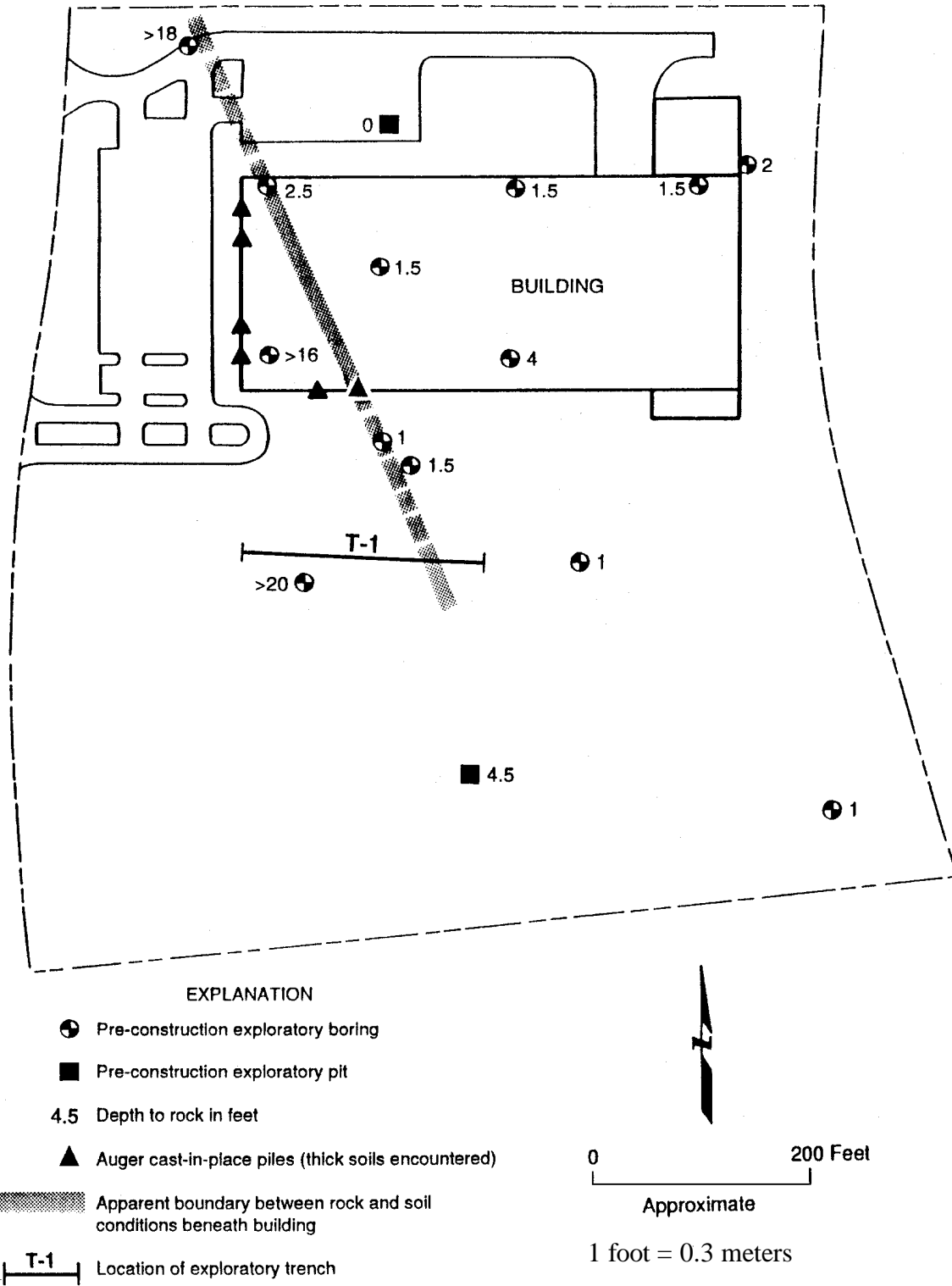


Figure G-1 Map of building site.

south of the building. The trench was sited to intersect the projected trend of the apparent linear soil/rock contact interpreted to lie beneath the western end of the building (Figure G-1). The walls of the trench were cleaned of the smeared soil coating, examined for evidence of faulting, and logged.

(1) The trench exposed no soil-bedrock contact. On the basis of the trench, it was concluded that the entire building is underlain by alluvial fan channel deposits consisting of cobbles and boulders of unweathered basalt in a fine-grained matrix. These hard channel deposits, which had a source east of the site, may have caused "refusal" during the pre-development geotechnical borings, leading to an interpretation that bedrock had been encountered in the easterly portion of the site. It was observed in the trench that the alluvial deposits became finer-grained toward the west. Toward the east, there was an increasing concentration of cobbles and boulders, reflecting the deposition of coarser material toward the upstream margin of the alluvial fan. The coarser materials in the eastern portion of the site were apparently interpreted as bedrock in the original geotechnical investigation. Examination of the trench did not reveal any evidence of faulting, and it was concluded that the potential for ground rupture due to faulting beneath the site was very low.

G-2. Example 2 - Liquefaction Hazard Screening

This example illustrates the steps involved in screening a site for liquefaction hazard using the criteria described in paragraph F-3. This example is based on a case history study for an existing building.

a. Review of available information

(1) Site development. The building site is located in a metropolitan area of a moderately-to-highly active tectonic region. The site development consists of two high-rise office buildings connected by an elevated bridge; both buildings were designed and constructed in the early-1970s. Each building is rectangular-shaped with a below-ground basement extending beneath the footprint of the building. Available drawings and plans for the buildings indicate that the structures are supported on systems of shallow foundations and footings situated beneath their respective basement-floor slabs. The foundation plans show the finished basement-floor slabs to be approximately 30 feet (9 m) below the existing grade adjacent to the building. The drawings and plans indicate that the footings of the perimeter walls are approximately 2.6 to 3.6 feet (0.3 to 1.1 m) below the finished basement-floor slab. The column footings for both buildings are typically square, with dimensions ranging between about 7 and 15 feet (2.1 and 4.6 m); the bottoms of these footings are generally about 5.5 to 7 feet (1.7 to 2.1 m) below the finished basement-floor slab, although some extend as deep as 11.5 to 13 feet (3.5 to 4 m).

(2) Soil conditions. The site is situated in an area mapped geologically as a Pleistocene-age formation, generally described as poorly consolidated, fine- to medium-grained sand and/or sandstone that was deposited in nearshore marine, lagoonal, and non-marine environments. Eleven soil borings drilled at the site during the buildings' original design phase encountered predominantly fine sand, silty fine sand, and fine sandy silt from the ground surface to the maximum exploration depth of about 63 feet (19.2 m). The logs of the soil borings indicate that beneath an approximately 3-foot (1-m) thick surficial veneer of sandy and clayey fill materials, the sands, silty sands, and sandy silts encountered within depths of about 15 feet (4.6 m) below the ground surface are loose to medium dense [$7 < (N_1)_{60} < 25$]. Underlying these near-surface sands and silts is a 12 to 15 foot (3.6 to 4.5 m) thick stratum of dense to very dense poorly graded fine- to medium-grained sand [$35 < (N_1)_{60} < 55$]. This sand stratum is in turn underlain by various thinner strata of generally dense to very dense sands, silty sands and occasional sandy silts [$30 < (N_1)_{60} < 60$], interbedded with very stiff to hard silty clays and clayey silts

extending at least to the penetration depth of the borings. The nature of the soil materials encountered in the borings is consistent with characteristics of the mapped geology.

(3) Groundwater conditions. Groundwater was encountered at the time of drilling the borings at depths varying between about 30 and 45 feet (9.1 and 13.7 m); it is not known to what extent, if any, tidal fluctuation affected this range of variation. Based on the available data, however, it is evident that groundwater elevations along the eastern boundary of the site are shallower than those in the western portions of the site by as much as about 6 to 8 feet (1.8 to 2.4 m).

(4) Topographic conditions. According to U.S. Geological Survey topographic maps and logs of soil borings drilled at the site during the design phase for the buildings, the ground surface across the site varies between elevations of about 25 and 34 feet (7.6 and 10.5 m) above mean sea level (MSL) and slopes very gently downward to the south at a gradient of less than a degree. The only significant topographic change in the site vicinity is at the waterfront along the bay situated approximately 2500 feet (750 m) to the south and west.

(5) Historic earthquake effects. The buildings, having been constructed in the early-1970s, have experienced only relatively distant, moderate- to large-magnitude earthquakes during their existence. The ground motions from such earthquakes have been merely felt in the site area, producing Modified Mercalli Intensity (MMI) V effects, and therefore have not been of consequence to the buildings or the site. During the historical time period prior to construction of the buildings (i.e. since about 1800), the site experienced ground shaking from several moderate to large earthquakes that reportedly produced MMI V-VII effects in the area. Two events in the nineteenth century, an estimated magnitude 6.5 in 1800 and an estimated magnitude 5.9 earthquake in 1862, reportedly produced MMI VII effects in the site area; both of these events are thought to have occurred on faulting in the offshore region west of the site area. There are no reports of ground failure distress for the site vicinity associated with these or other historic earthquakes.

b. Liquefaction hazard screening

(1) Susceptibility. Based upon review of the available geologic information, the site is underlain by Pleistocene-age deposits with soil-like characteristics, rather than rock-like characteristics. Although the liquefaction susceptibility of the deposits is probably not greater than low according to Table F-1, the deposits cannot be categorically rated as having a very low susceptibility; therefore, liquefaction hazard cannot be screened out on the basis of the susceptibility criterion.

(2) Groundwater. The groundwater table at the site was encountered at depths between about 30 and 45 feet (9.1 and 13.7 m). These depths are less than 50 feet (15 m) below the ground surface; therefore, liquefaction hazard cannot be screened out on the basis of the groundwater depth.

(3) Soil conditions. The available logs of borings drilled at the site indicate that predominantly fine sand, silty fine sand, and fine sandy silt (cohesionless) deposits underlie the site and the reported penetration resistance (blowcount) data suggest that these deposits vary in compactness from loose to very dense. The loose to medium dense [i.e., $(N_I)_{60} < 30$] deposits were encountered at shallow depths within the profile, well above the groundwater table; whereas, the cohesionless deposits situated below the groundwater table are dense to very dense [i.e., $(N_I)_{60} > 30$]. Additionally, the silty clay and clayey silt strata interbedded with the deeper cohesionless deposits are described as very stiff to hard. On the basis of these soil conditions, the screening criteria indicate that the liquefaction hazard at the site is not significant and that the site may be eliminated from further liquefaction evaluation.

G-3. Example 3 - Liquefaction Potential Evaluation

a. Introduction

This example illustrates the steps involved in evaluating liquefaction potential using the Seed-Idriss empirically based methodology described in paragraph F-4. This procedure is a widely used procedure that would typically be employed for a site for which there remains the potential for a liquefaction hazard after applying the screening criteria in paragraph F-3. Also included in this example is an assessment of the consequences of liquefaction in terms of settlements.

(1) The site conditions are illustrated in Figure G-2. Approximately 50 feet (15 m) of predominantly loose to medium dense sand with lenses of clay of Holocene geologic age overlies dense (non liquefiable) sands and stiff clays. The water table is at a depth of 20 feet (6.1 m). The site cannot be screened out as having an insignificant potential for liquefaction using any of the three criteria given in paragraph F-3; therefore, the soils below 20 feet (6.1 m) depth are evaluated for their liquefaction potential and consequences. The soils above the water table cannot be screened out for differential compaction using the criteria in paragraph F-3; therefore, settlements in the upper 20 feet (6.1 m) are evaluated also.

(2) The proposed structure is a light, two-story structure to be supported on isolated spread footings bearing at a depth of 2 feet (0.6 m) below the ground surface. Because the foundation loads are light and the footings are well above the water table, there is not a potential for liquefaction to result in a foundation bearing capacity failure. Rather, the primary concern is settlement due to consolidation of the liquefied sand as pore pressures dissipate following liquefaction. The sands above the water table may also densify due to the ground shaking and contribute to the overall settlement. Settlements are estimated using the Tokimatsu and Seed (1987) methods. The site and vicinity is flat, with a slope gradient of less than 0.1 percent, and there are no free faces within thousands of meters of the site. The potential for lateral spreading movements is therefore judged to be negligible.

b. Liquefaction potential

A plot of the Standard Penetration Test (SPT) blowcounts (N-values) in sands versus depth is shown in Figure G-3. These blowcounts were obtained in borings using recommended methods described in Seed et al. (1985) and Youd and Idriss (1997) and no energy correction to the values is required. For assessment of

liquefaction potential, the N-values are converted or normalized to $(N_I)_{60}$ values. This involves adjusting the values to a common effective overburden pressure of 1 tsf (96 kPa) using the relationship in Figure G-4. The calculations for each of the five borings drilled at the site are shown in Table G-1. The sands at the site contain varying amounts of silty fines (i.e., the percentage of minus No. 200 sieve material). The percentage of fines influences the liquefaction susceptibility, as shown in Figure G-5 (Youd and Idriss, 1997; Seed et al., 1985), which will be used to assess the liquefaction potential. For this evaluation, it is desired to use the correlation curve for clean sands (# 5 percent fines) in Figure G-5. Therefore, it is necessary to further adjust the $(N_I)_{60}$ values of the silty sands (> 5 percent fines) to a clean sand condition. The following equations are utilized to make this adjustment in the $(N_I)_{60}$ values:

$$(N_I)_{60cs} = a + b(N_I)_{60}$$

where:

$$\begin{aligned} \alpha &= 0 && \text{for FC}\#5\% \\ \alpha &= \exp[1.76-(190/FC^2)] && \text{for } 5\% < \text{FC} < 35\% \\ \alpha &= 5.0 && \text{for FC}\geq 35\% \end{aligned}$$

$$\begin{aligned} \beta &= 1.0 && \text{for FC}\#5\% \\ \beta &= [0.99+(FC^{1.5}/1000)] && \text{for } 5\% < \text{FC} < 35\% \\ \beta &= 1.2 && \text{for FC}\geq 35\% \end{aligned}$$

where FC is the fines content (expressed as a percentage) measured from laboratory gradation tests from retrieved soil samples.

The adjusted $(N_I)_{60}$ clean-sand values are shown in the right-hand column of Table G-1 and plotted versus depth in Figure G-6.

(1) The next step is to assess the "critical" $(N_I)_{60}$ values for the site, i.e. the $(N_I)_{60}$ values dividing expected liquefaction and non-liquefaction behavior. To accomplish this, the cyclic stress ratio, t_a/s'_o , induced in the soil by the earthquake ground shaking is calculated as a function of depth for depths below the ground water table. The simplified procedure developed by Seed and Idriss (1971) is used to

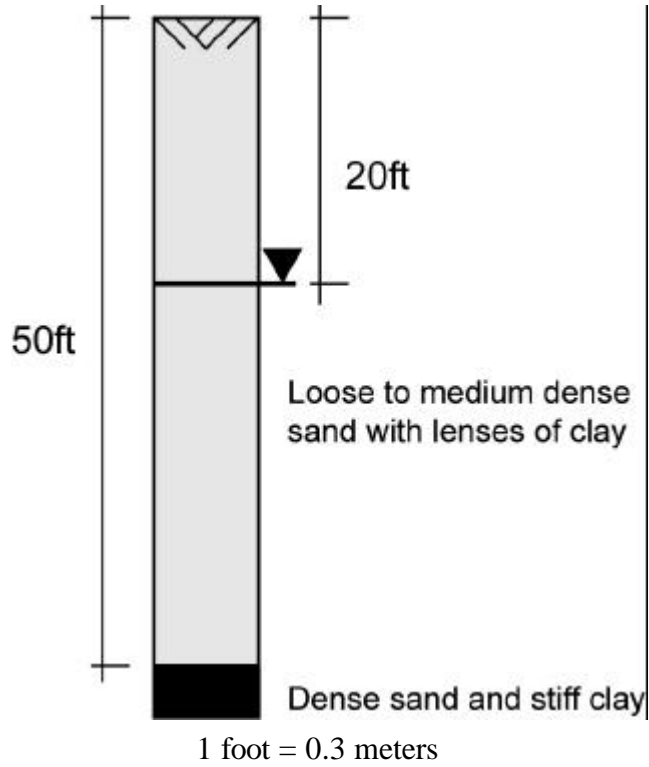


Figure G-2 Site soil profile.

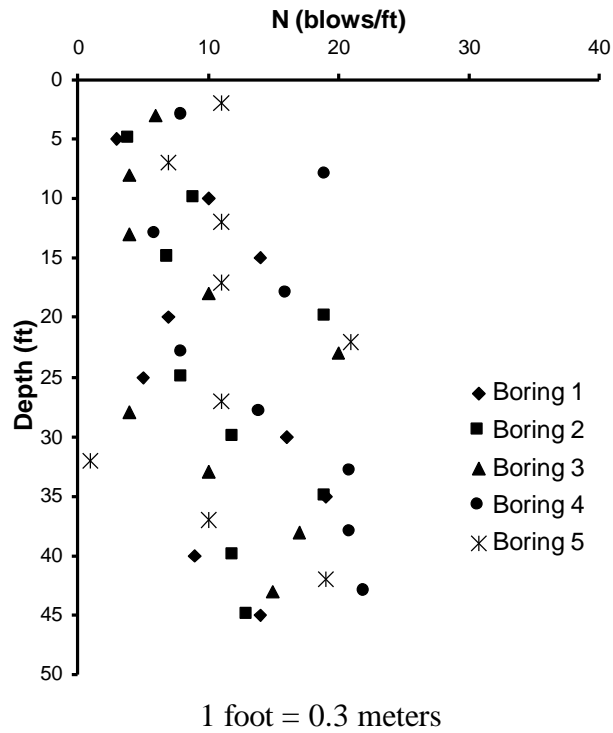


Figure G-3 Plot of SPT blowcounts vs. depth.

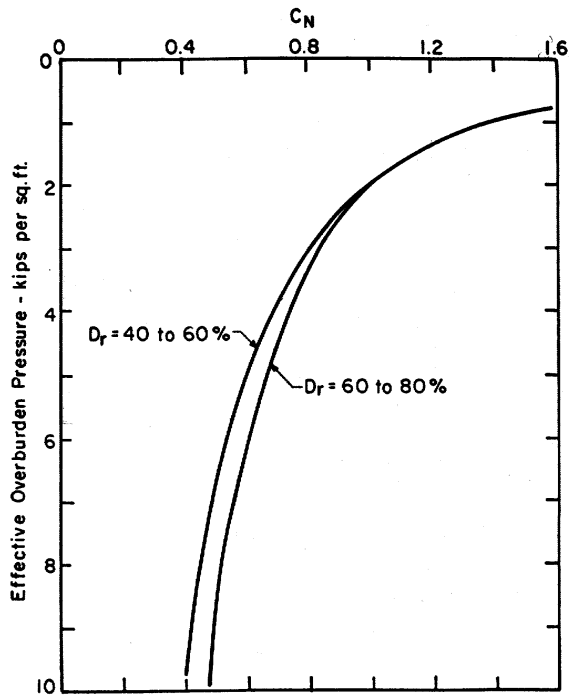


FIG. 4.—Chart for Values of C_N

1 ksf = 47.9 kPa

Figure G-4 Relationship between C_N and S_o' (from Seed et al., 1985).

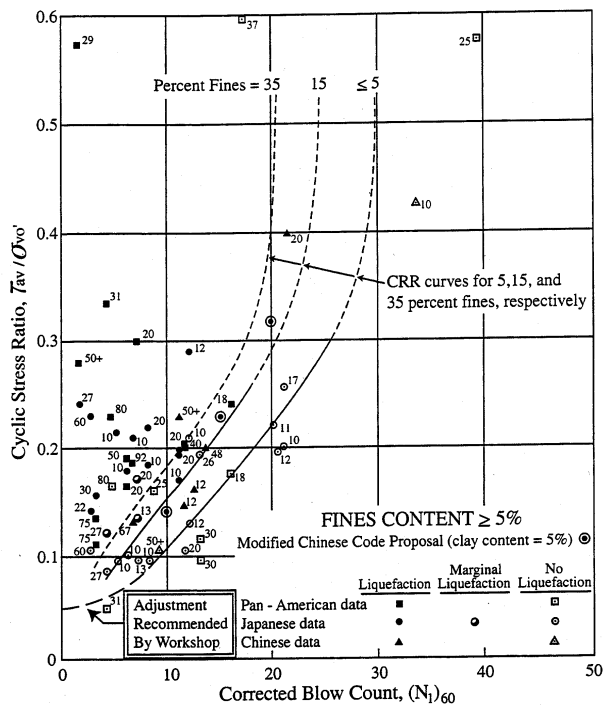


Figure G-5 Relationship between cyclic stress ratio (CSR) causing liquefaction and $(N_1)_{60}$ (from Seed et al., 1985; Youd and Idriss, 1997).

Table G-1 Calculation of the $(N_1)_{60\text{ cs}}$ values.

Boring 1							
Depth	S_o	S_o'	N	C_N	$(N_1)_{60}$	Fines Content	$(N_1)_{60\text{ cs}}$
ft	psf	psf	blows/ft		blows/ft	%	blows/ft
5	575	575	3	1.60	5	10	6
10	1150	1150	10	1.26	13	5	13
15	1725	1725	14	1.05	15	2	15
20	2300	2300	7	0.90	6	15	9
25	2875	2563	5	0.86	4	3	4
30	3450	2826	16	0.82	13	8	13
35	4025	3089	19	0.78	15	5	15
40	4600	3352	9	0.75	7	7	7
45	5175	3615	14	0.71	10	9	11

Boring 2							
Depth	S_o	S_o'	N	C_N	$(N_1)_{60}$	Fines Content	$(N_1)_{60\text{ cs}}$
ft	psf	psf	blows/ft		blows/ft	%	blows/ft
5	575	575	4	1.60	6	12	8
10	1150	1150	9	1.26	11	4	11
15	1725	1725	7	1.05	7	8	7
20	2300	2300	19	0.90	17	10	18
25	2875	2563	8	0.86	7	2	7
30	3450	2826	12	0.82	10	7	10
35	4025	3089	19	0.78	15	4	15
40	4600	3352	12	0.75	9	15	12
45	5175	3615	13	0.71	9	3	9

Boring 3							
Depth	S_o	S_o'	N	C_N	$(N_1)_{60}$	Fines Content	$(N_1)_{60\text{ cs}}$
ft	psf	psf	blows/ft		blows/ft	%	blows/ft
3	345	345	6	1.60	10	10	11
8	920	920	4	1.45	6	7	6
13	1495	1495	4	1.13	5	3	5
18	2070	2070	10	0.97	10	15	13
23	2645	2458	20	0.88	18	4	18
28	3220	2721	4	0.84	3	20	7
33	3795	2984	10	0.80	8	8	8
38	4370	3247	17	0.75	13	2	13
43	4945	3510	15	0.73	11	6	11

Table G-1 Calculation of the $(N_1)_{60\text{ cs}}$ values. (continued)

Boring 4							
Depth	S_o	S_o'	N	C_N	$(N_1)_{60}$	Fines Content	$(N_1)_{60\text{ cs}}$
ft	psf	psf	blows/ft		blows/ft	%	blows/ft
3	345	345	8	1.60	13	5	13
8	920	920	19	1.45	28	9	29
13	1495	1495	6	1.13	7	14	10
18	2070	2070	16	0.97	16	2	16
23	2645	2458	8	0.88	7	7	7
28	3220	2721	14	0.84	12	3	12
33	3795	2984	21	0.80	17	5	17
38	4370	3247	21	0.75	16	17	20
43	4945	3510	22	0.73	16	6	16

Boring 5							
Depth	S_o	S_o'	N	C_N	$(N_1)_{60}$	Fines Content	$(N_1)_{60\text{ cs}}$
ft	psf	psf	blows/ft		blows/ft	%	blows/ft
2	230	230	11	1.60	18	7	18
7	805	805	7	1.50	11	15	14
12	1380	1380	11	1.20	13	3	13
17	1955	1955	11	1.00	11	7	11
22	2530	2405	21	0.91	19	15	22
27	3105	2668	11	0.84	9	4	9
32	3680	2931	1	0.81	1	9	2
37	4255	3194	10	0.77	8	13	10
42	4830	3457	19	0.74	14	2	14

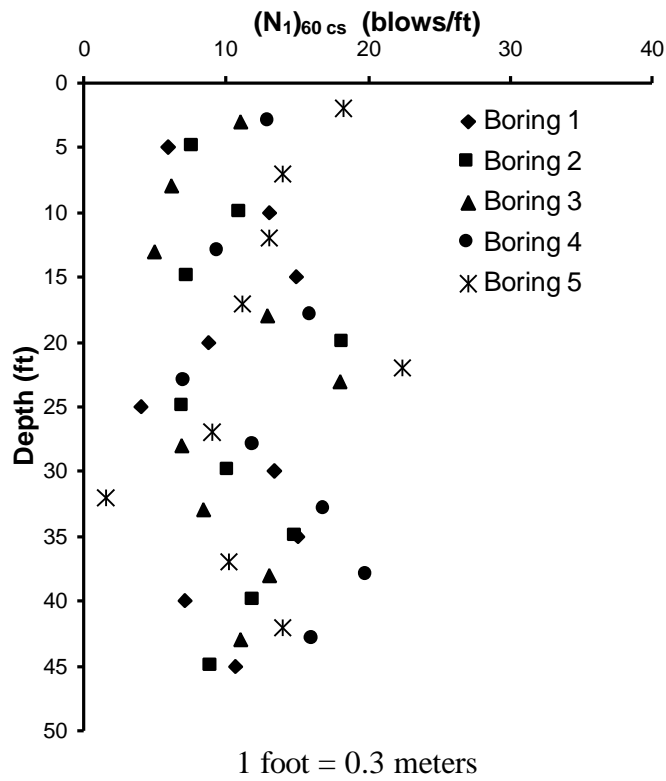


Figure G-6 Plot of $(N_1)_{60 cs}$ vs. depth.

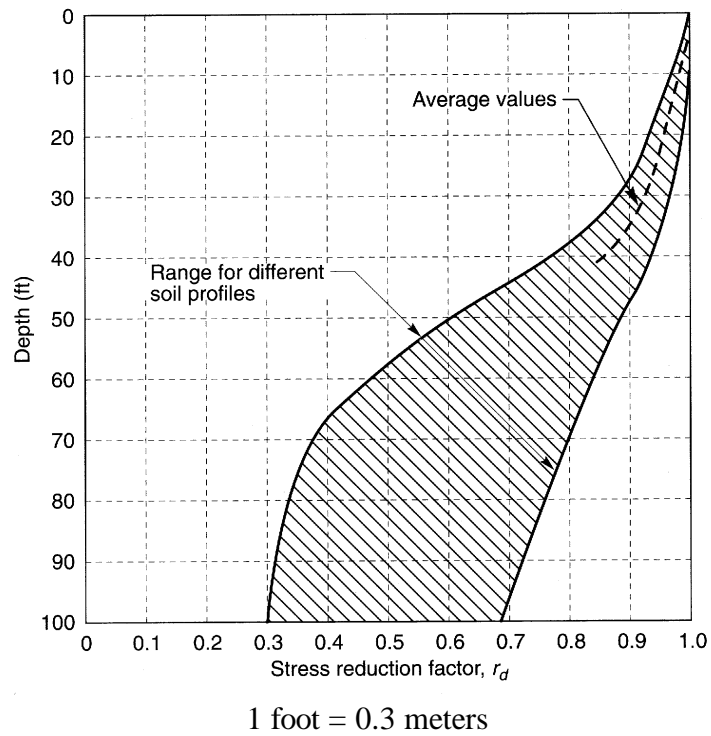


Figure G-7 Relationship between r_d and depth (from Seed and Idriss, 1971).

calculate the cyclic stress ratio, as follows (Seed and Idriss, 1971; Seed et al., 1985):

$$CSR = \frac{t_a}{s'_o} = 0.65 \frac{a_{\max}}{g} \cdot \frac{s_o}{s'_o} \cdot r_d$$

where a_{\max} is the free field surface peak ground acceleration, which is equal to 0.25g for this example problem, s_o is to total vertical stress at depth z , s'_o is the effective vertical stress at depth z , and r_d is a stress reduction factor with values given by Figure G-7. The first five columns of Table G-2 show the calculation of induced cyclic stress ratio, t_a/s'_o . Having this stress ratio, Figure G-5 is used to obtain the corresponding values of critical $(N_I)_{60}$ from the CRR curve for clean sands (# 5 percent fines). This curve is approximated by the following equation:

$$CRR_{7.5} = \frac{a + cx + ex^2 + gx^3}{1 + bx + dx^2 + fx^3 + hx^4} \text{ for } x < 30$$

where:

$$\begin{aligned} a &= 0.048 \\ b &= -0.1248 \\ c &= -0.004721 \\ d &= 0.009578 \\ e &= 0.0006136 \\ f &= -0.0003285 \\ g &= -0.00001673 \\ h &= 0.000003714 \\ x &= (N_I)_{60cs} \end{aligned}$$

However, for this site, the peak ground acceleration of 0.25g is caused by a magnitude 6.75 earthquake, whereas the curve in Figure G-5 is for a magnitude 7.5 earthquake. Therefore the curve needs to be adjusted to a magnitude 6.75 condition using the factors in Table F-2 (Seed and Idriss, 1982; Seed et al., 1983, 1985). The adjustment factor to the ordinate of the curve is 1.13. This factor, denoted K_m , is shown in Column VI of Table G-2. A further adjustment of the curves has been recommended by Seed and Harder (1990) to account for the possible reduction in values of t_a/s'_o causing liquefaction if values of the effective overburden pressure, s'_o , exceed 1 tsf (96 kPa). Their recommended adjustment factors, K_s , are shown in Figure G-8 and are a function of s'_o . Column VII in Table G-2 shows the K_s factors. Column VIII shows the critical $(N_I)_{60}$ values for a magnitude 7.5 earthquake and s'_o equal to 1 tsf (96 kPa). Column IX shows the

final critical $(N_I)_{60}$ values for the design earthquake of magnitude 6.75 and the site values of s'_o . For the linear portions of the curve in G-5, the final critical $(N_I)_{60}$ values are obtained as:

$$(N_I)_{60critical}(M 6.75, s'_o) = \frac{(N_I)_{60critical}(M 7.5, s'_o = 1tsf)}{K_m \cdot K_s}$$

(2) The critical $(N_I)_{60}$ curve is superimposed on the $(N_I)_{60}$ data in Figure G-9. Most of the data lie to the left of the curve, indicating liquefaction is likely to occur.

c. Settlement

The next step is to estimate the settlement of the soils below 20 feet (6.1 m) depth and also associated with the compaction of the soils above 20 feet (6.1 m) depth. The procedures presented in Tokimatsu and Seed (1987) are used. The Tokimatsu and Seed correlation for volumetric strain (percent settlement) of saturated clean sand for a magnitude 7.5 earthquake is shown in Figure G-10. The correlation is similar to that for liquefaction shown in Figure G-5. For a magnitude 6.75 earthquake, the curves in Figure G-10 are adjusted upward by the factor K_m equal to 1.13. The $(N_I)_{60}$ data below the water table average about 10 blows/0.3 m (10 blows/foot) (Figure G-9). The induced cyclic stress ratio below the water table is in the range of about 0.16 to 0.19 (Table G-2). Comparing this stress ratio and a value of $(N_I)_{60}$ equal to 10 blows/foot with curves in Figure G-10 (after adjusting them upward by a factor of 1.13) indicates a volumetric strain of about 2.5 percent. Thus, for a 30-foot (9.1 m) thickness of liquefied sand, the estimated settlement is 0.025 x 30 feet (9.1 m) = 9 inches (23 cm).

(1) Estimates of settlements in the upper 20 feet (6.1 m) of sands above the water table are made using the procedures described in Tokimatsu and Seed (1987). The first step is to calculate the shear strain developed in the soils using the relationship:

$$\mathbf{g}_{eff} \left(\frac{G_{eff}}{G_{\max}} \right) = \frac{0.65 \cdot a_{\max} \cdot s_o \cdot r_d}{g \cdot G_{\max}}$$

Table G-2 Calculation of CSR and $(N_1)_{60}$ critical.

Water Table at 20 ft	Design Earthquake:
$\gamma_t = 115$ pcf	PGA = 0.25 g
	$M_w = 6.75$

Depth	S_o	S_o'	r_d	CSR	K_m	K_s	$(N_1)_{60 cr}$ M = 7.5	$(N_1)_{60 cr}$ M = 6.75
ft	psf	psf					blows/ft	blows/ft
I	II	III	IV	V	VI	VII	VIII	IX
5	575	575	0.99	0.16	1.13	N/A	N/A	N/A
10	1150	1150	0.98	0.16	1.13	N/A	N/A	N/A
15	1725	1725	0.97	0.16	1.13	N/A	N/A	N/A
20	2300	2300	0.95	0.15	1.13	0.99	14.2	12.7
22.5	2588	2432	0.95	0.16	1.13	0.99	15.0	13.5
25	2875	2563	0.94	0.17	1.13	0.98	15.8	14.3
27.5	3163	2695	0.93	0.18	1.13	0.97	16.4	15.0
30	3450	2826	0.92	0.18	1.13	0.96	17.0	15.7
32.5	3738	2958	0.91	0.19	1.13	0.94	17.2	16.2
35	4025	3089	0.90	0.19	1.13	0.93	17.3	16.4
37.5	4313	3221	0.87	0.19	1.13	0.92	17.4	16.7
40	4600	3352	0.85	0.19	1.13	0.92	17.4	16.8
42.5	4888	3484	0.82	0.19	1.13	0.91	17.4	16.9
45	5175	3615	0.80	0.19	1.13	0.90	17.3	17.1
47.5	5463	3747	0.77	0.18	1.13	0.89	17.2	17.1

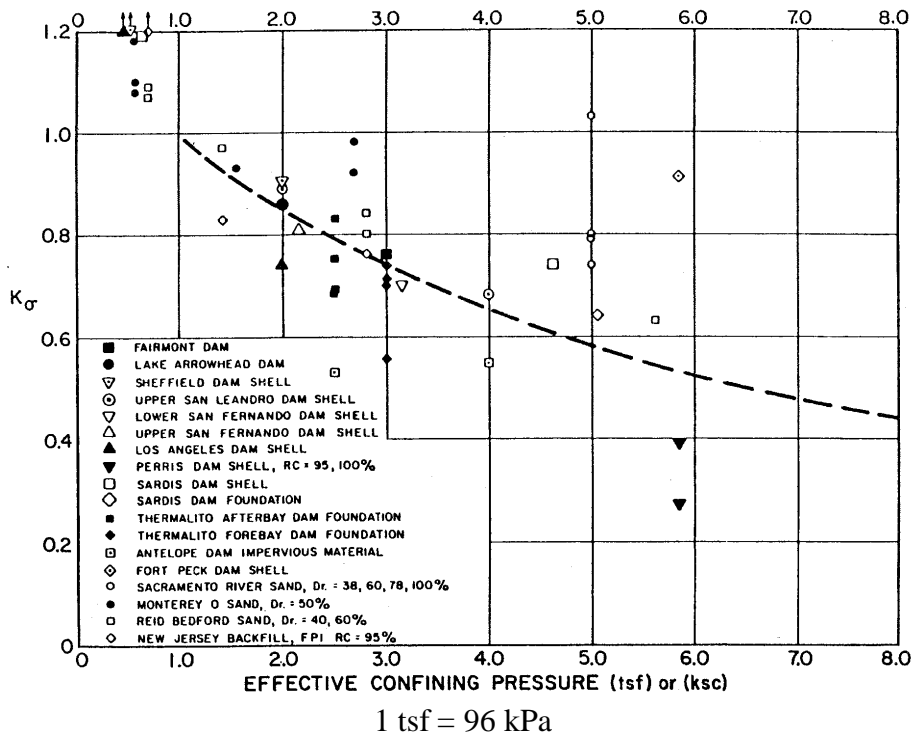


Figure G-8 Relationship between K_s and S_0' (from Seed and Harder, 1990).

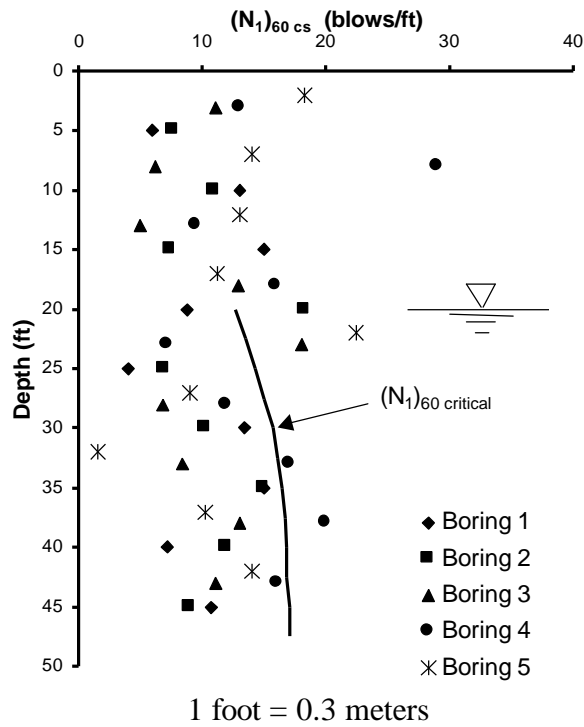


Figure G-9 $(N_1)_{60 \text{ critical}}$ superimposed on $(N_1)_{60 \text{ cs}}$ data with depth.

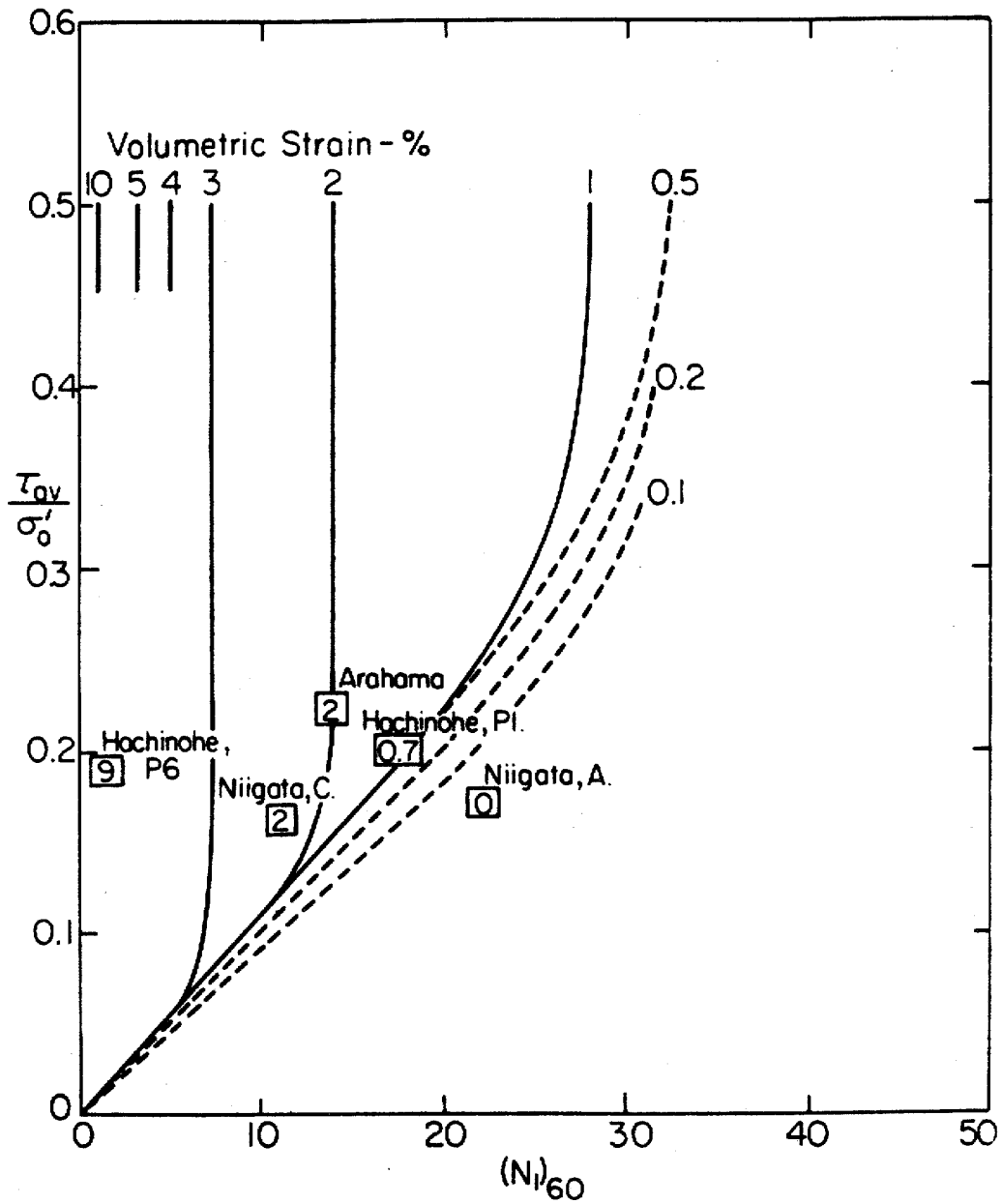


Figure G-10 Correlation for volumetric strain, cyclic stress ratio (CSR), and $(N_1)_{60}$ for sands (from Tokimatsu and Seed, 1987).

in which γ_{eff} is the effective average shear strain induced in the soil at a certain depth by the design earthquake ground shaking, G_{eff} is the shear modulus at this strain level, and G_{max} is the maximum shear modulus at a very low strain. This calculation is made for three soil layers in the upper 20 feet (6.1 m) in Table G-3. Then, using Figure G-11, γ_{eff} is obtained for the respective values of effective overburden pressure. From Figure G-12, the volumetric strains or percent settlements are obtained for the effective shear strain in each layer using an average $(N_1)_{60}$ value equal to 10 blows/0.3 m (10 blows/foot) in the upper 20 feet (6.1 m). These volumetric strains are for magnitude 7.5 and should be reduced for the shorter duration of shaking for magnitude 6.75 using Table G-4. Finally, the correlations in Figure G-12 are based on unidirectional shaking, and research by Pyke, et al. (1975) indicates that the volumetric strains due to multidirectional shaking are about twice those for unidirectional shaking. Therefore, the volumetric strains are doubled. The sum of the estimated settlements in the upper 20 feet (6.1 m) is only 0.3 inches (0.7 cm), which is additive to the 9 inches (23 cm) of settlement due to liquefaction of the underlying sands, leading to a total estimated settlement of about 9.2 inches (24 cm) beneath the building. (Note that the settlement estimates for the sand above the water table are sensitive to the level of acceleration. For example, the calculated settlements in the upper 20 feet (6.1 m) would increase from only 0.3 inches (0.7 cm) to approximately 1.6 inches (4 cm) if the peak ground acceleration increased from 0.25g to 0.50g, yet the settlements associated with liquefaction 20 feet (6.1 m) in depth would not change as long as liquefaction occurs.)

(2) Consideration of the sand variability from boring to boring as well as varying thicknesses of the sand due to presence of clay lenses across the site would lead to estimates of differential settlements between footings. If these would lead to unacceptable structural distress, then alternative mitigation measures (described in paragraph F-5) would include: (1) densifying the soils; (2) grouting the soils; (3) installing permeable drainage columns; (4) installing a permanent dewatering system to lower the ground water table to the base of the liquefiable layer (note that the effects of this method in causing consolidation of shallow clay lenses and deeper clay strata would have to be evaluated); (5) using pile or pier foundations to extend below the liquefiable layer; and (6) stiffening the foundation system by tying isolated footings together with well-reinforced grade beams or mats.

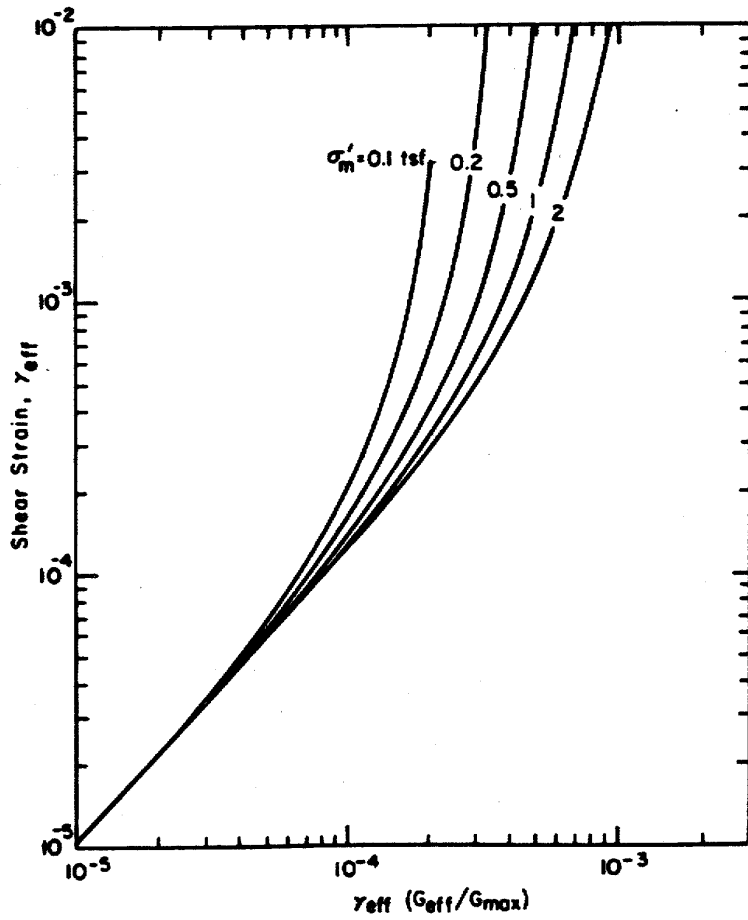


Figure G-11 Plot of induced shear strain for sands (from Tokimatsu and Seed, 1987).

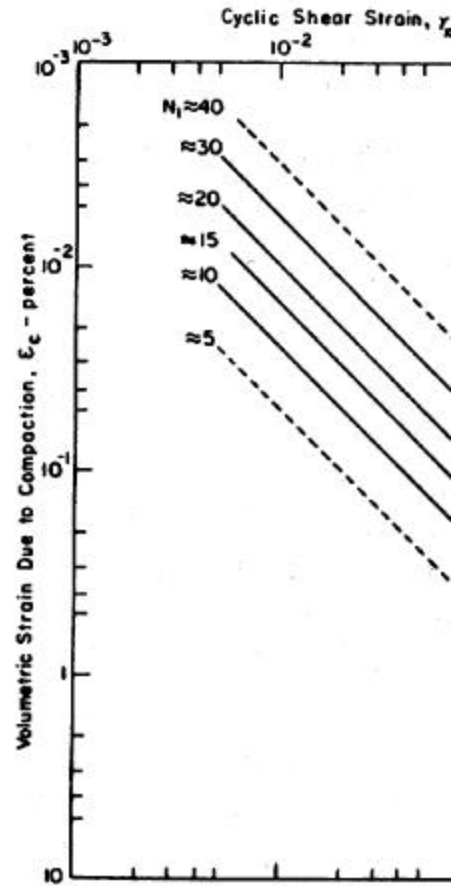


Figure G-12 Correlation for volumetric strain and $(N_1)_{60}$ (from Tokimatsu and Seed, 1987).

Table G-3 Calculation of settlement of sand above ground water table.

Water Table at 20 ft $\gamma_t = 115$ pcf	Design Earthquake: PGA = 0.25 g $M_w = 6.75$
--	--

Depth	Thickness	S_o	r_d	N_1	G_{max}^1	σ_{eff}	σ_{eff}	$e_v, M_w=7.5$	$e_v, M_w=6.75$	2
ft	ft	psf			psf	(G_{eff}/G_{max})		%	%	
5	7.5	575	0.99	10	8.44E+05	1.1E-04	2.2E-04	0.05	0.04	
10	5	1150	0.98	10	1.19E+06	1.5E-04	2.8E-04	0.07	0.06	
15	7.5	1725	0.97	10	1.46E+06	1.9E-04	3.4E-04	0.09	0.08	
¹ : $G_{max} = 20 * (N_1)^{1/3} * (S_m)^{1/2} * 1000$										Total :

G-18

Table G-4 Scaling factors for influence of earthquake magnitude on volumetric strain for dry sand (Seed, 1987).

Earthquake Magnitude	$e_{M=m} / e_{M=7.5}$
M_w	
8½	1.25
7½	1.00
6:	0.85
6	0.60
53	0.40

G-4. Example 4 – Landslide Hazard Screening

This example presents the steps involved in screening a site for potential earthquake-induced landsliding hazards. The example problem is illustrated in Figure G-13.

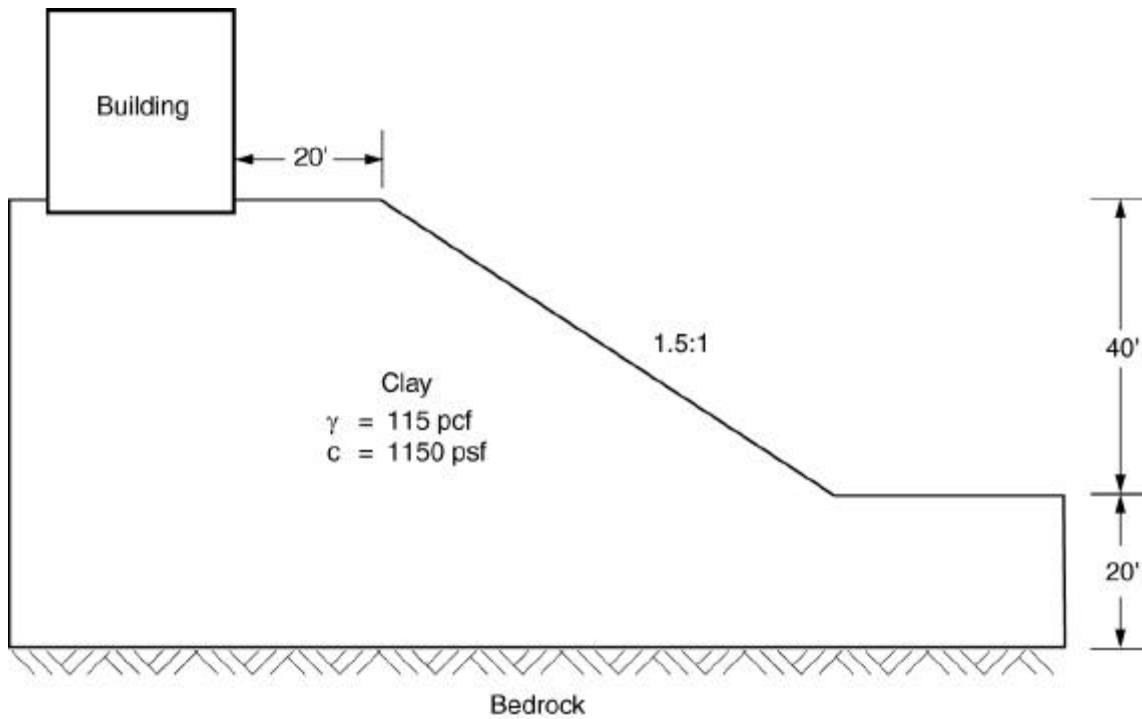
a. Review of available information

(1) Site development and soil conditions. A barracks building is located 20 feet (6.1 m) back from the crest of a 40 feet (12 m) high slope (Figure G-13). The ratio of the slope width to the slope height is approximately 1.5:1. The building is to be supported on a shallow foundation system. Soil conditions at the site consist of clay with a uniform undrained shear strength (cohesion) of approximately 1150 psf (55.2 kPa) and a unit weight of 115 pcf (18.0 kN/m³). Bedrock is located approximately 60 feet (18 m) below the building and groundwater is not present at the site.

(2) Historic earthquake effects and postulated earthquake parameters. This site has been shaken by several moderate earthquakes. However, no known historic information indicates that earthquake-induced landsliding occurred. Inspection of the building site shows that the slope is stable under static conditions. No cracking above the slope crest or other evidence of present instability were observed. Seismic landslide hazard maps have not been developed for this area. Site specific analyses determined the MCE to have a moment magnitude of approximately 6.5 and a peak horizontal acceleration of 0.40 g. The predominant period of the induced acceleration time-history, T_o , was estimated to be 0.3 seconds.

b. Earthquake-induced landslide screening

(1) Susceptibility. To conclude that a landsliding hazard does not, each of the landslide screening criteria presented in paragraph F-3 must be satisfied. The stability of the slope during past earthquakes and present site conditions indicate no significant susceptibility to landsliding. The site is not adjacent to a shoreline. The building is located approximately 20 feet (6.1 m) from the top of the slope and a horizontal distance of 80 feet (24 m) from the toe of the slope (Figure G-13). According to the screening criteria, the building cannot be located closer than the distance of the slope height (40 feet or 12 m) from the top of the slope or closer than three times the slope height (120 feet or 37 m) from the toe of the slope. This criterion is not satisfied indicating further evaluation is required.



1 foot = 0.3 meters; 1 pcf = 0.16 kN/m³; 1 psf = 48 Pa

Figure G-13 Profile of earthquake-induced landsliding example problem.

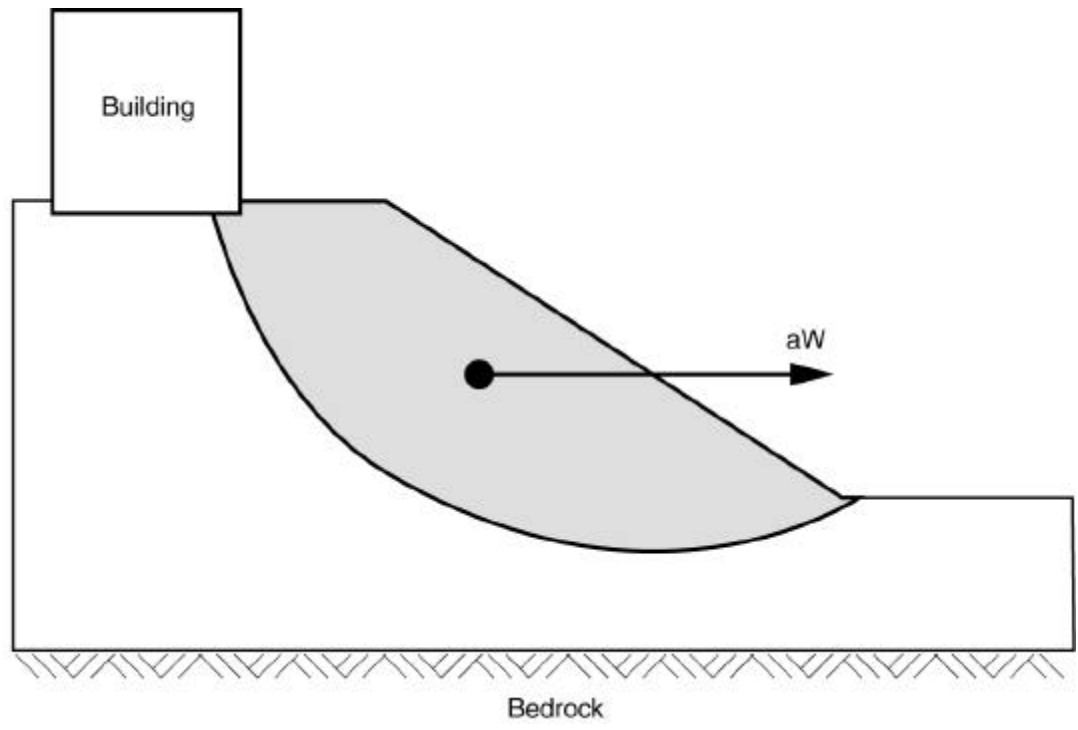


Figure G-14 Failure surface and pseudo-static load for earthquake-induced landsliding example problem.

G-5. Example 5 - Landslide hazard evaluation

The general method for evaluating the seismic stability of slopes involves both pseudo-static and deformation analysis procedures, as illustrated below.

a. Pseudo-static slope stability analysis

Pseudo-static slope stability analyses conservatively evaluate the occurrence of a slope failure due to earthquake loading. If the results of the pseudo-static analysis indicate potential deformation of the slope (factor of safety < 1), a deformation analysis is performed to estimate the displacement. A static limit-equilibrium slope stability analysis performed for the site determined that the critical failure surface would intersect the foundation of the building (Figure G-14). This failure surface was then used for the pseudo-static slope stability analysis. The seismic coefficient was assumed to be equal to the peak horizontal acceleration of 0.40 g. The results of the pseudo-static analysis indicate a marginal susceptibility to earthquake-induced landsliding with a factor of safety of 0.92. A deformation analysis was then performed to estimate the displacement.

b. Deformation analysis

The deformation analysis procedure is based on Newmark's (1965) concept of yield acceleration. For a specified potential sliding mass, the acceleration induced by the earthquake is compared with the yield acceleration. When the induced acceleration exceeds the yield acceleration, downslope movements will occur along the direction of the assumed failure plane. The movement will stop when the induced acceleration drops below the yield acceleration.

(1) Yield acceleration, k_y . The yield acceleration is the acceleration at which the potential sliding surface would develop a factor of safety of unity. For this site, k_y was determined to be 0.30 g by iteratively adjusting the seismic coefficient in the pseudo-static analysis until the factor of safety reached a value of unity.

(2) Peak or maximum acceleration, k_{max} . This parameter represents the peak or maximum acceleration induced within the sliding mass. k_{max} was assumed to be equal to the peak horizontal acceleration of 0.40 g.

(3) Acceleration ratio. The acceleration ratio is calculated by dividing the yield acceleration, k_y , by the maximum acceleration, k_{max} . For this example, the acceleration ratio is equal to 0.75.

(4) Deformation. Several simplified methods based on the concept of yield acceleration originally proposed by Newmark (1965) are utilized to estimate deformation.

- (a) Makdisi and Seed (1978). The Makdisi and Seed (1978) method normalizes displacement by k_{max} , T_o , and gravity (Figure F-17). Based on the ratio of k_y to k_{max} of 0.75 and a moment magnitude of 6.5, the normalized displacement is equal to approximately 0.003 seconds (note that the units of seconds will be replaced by inches when the normalizing values are factored out). An estimated deformation of 0.14 inches (0.4 cm) was calculated by multiplying the normalized displacement by the values of k_{max} , T_o , and gravity.
- (b) Egan (1994). The Egan (1994) relationship between deformation and the ratio of critical acceleration is normalized by k_{max} and the number of earthquake cycles. A magnitude 6.5 earthquake contains approximately eight cycles (Figure F-18a). Based on the ratio of k_y to k_{max} of 0.75, the displacement factor was estimated to be 0.3 (Figure F-18b). An estimated deformation of 0.4 inches (1 cm) was determined by multiplying the displacement factor by the values of k_{max} and the number of cycles.
- (c) Franklin and Chang (1977). The range of the Franklin and Chang (1977) simplified method has a lower bound of one inch of deformation (Figure F-19). The critical acceleration ratio of 0.75 is outside this range. However, judging from the trend of the curves, a deformation of less than one inch (2.5 cm) can be assessed.
- (d) Yegian et al. (1991). The Yegian et al. (1991) simplified method for estimating permanent deformation normalizes displacement by k_{max} , T_o^2 , number of cycles, and gravity (Figure F-20). A magnitude 6.5 earthquake contains approximately eight cycles (Figure F-18a). Based on the ratio of k_y to k_{max} of 0.75, the normalized permanent deformation was estimated to be 0.001. An estimated deformation of 0.1 inches (0.03 cm) was determined by multiplying the normalized displacement value of 0.001 by the values of k_{max} , T_o^2 , number of cycles, and gravity.

c. Hazard mitigation

The amount of acceptable deformation is dependent on several factors including: foundation rigidity, age of the building, building function, regulatory requirements, and economic alternatives. For this example problem, each deformation analysis method predicted less than one inch (2.5 cm) of displacement. This magnitude of displacement was determined to be acceptable considering the use and structural characteristics of the building. Thus, stabilization methods were not needed at this site.